Automotive Experiences
Vol. 7 No. 3 (2024) pp. 567-578
p-ISSN: 2615-6202 e-ISSN: 2615-6636

Research Paper

Crashworthiness Performance Study of 3D-Printed Multi-Cell Tubes Hybridized with Aluminum Under Axial Quasi-Static Testing

Riki Ardiansyah[1], Fitri Karina Indriani[2], Dony Hidayat[3], Arif Tjahjono[2], Abian Nurrohmad[1], Aryandi Marta[1]

1Research Center for Aeronautics Technology, National Research and Innovation Agency – BRIN, Bogor 16350, Indonesia
[2]Department of Material Physics, Universitas Islam Negeri Syarif Hidayatullah, Tangerang Selatan 15412, Indonesia
[3]Department of Mechanical, Faculty of Engineering, Universitas Indonesia, Depok 16424, Indonesia

riki005@brin.go.id

https://doi.org/10.31603/ae.12247

Published by Automotive Laboratory of Universitas Muhammadiyah Magelang

Article Info
Submitted: 06/09/2024
Revised: 17/10/2024
Accepted: 06/11/2024
Online first: 14/12/2024

Abstract

This study investigates the crashworthiness performance of 3D-printed hybrid tubes, fabricated using PLA and PACF filaments with varying shell thicknesses (1, 1.5, and 2 mm). The hybrid tubes, composed of a shell, aluminum, and multi-cell structure, were subjected to axial quasi-static testing. Results indicate that both shell thickness and filament type significantly influence crashworthiness. PLA specimens with a shell thickness of 2 mm absorbed 504 J of energy, whereas PACF specimens with the same thickness absorbed only 342.9 J. The deformation mode analysis revealed mixed deformation patterns, including diamond, fracture, and fragmented modes. The study also evaluated specific energy absorption (SEA) and crushing force efficiency (CFE). The PLA specimen with a 2 mm shell thickness exhibited the highest SEA value of 18.61 J/g among all specimens. In contrast, the PACF specimen with the same shell thickness demonstrated the highest CFE value of 0.82 among the tested specimens. Overall, this research contributes insights into the design optimization of 3D-printed hybrid tubes for enhanced crashworthiness.

Keywords: Crashworthiness; Hybrid Tubes; 3D Printing; Energy Absorption; Deformation

1. Introduction

One of the major issues that concern many countries internationally is traffic accidents. A car crash results in injuries or fatalities to [1]–[6]. There are several approaches used to improve driving safety. It is widely recognized that having thin structures that can be sacrificed to absorb impact energy increases vehicle safety (crashworthiness) [7], [8]. Crashworthiness is the ability of a vehicle's structure to deform in a controlled manner, providing sufficient space for occupants and thereby limiting the potential for injuries during a crash event [9]. The crashworthiness testing serves as a preventive measure to mitigate the occurrence of fatalities and injuries among passengers. The development of energy-absorbing structures has been implemented in thin-walled metal structures across various industries such as automotive [10], [11], railway [12], aerospace [13], and shipbuilding [14].

Building on this, many researchers have explored energy absorbers with various structural design configurations to achieve optimal crashworthiness values while keeping the mass as light as possible. The evolution of structural configurations began with simpler forms such as circular tubes, square tubes, and triangular tubes, as demonstrated by Baroutaji et al. [15]. Over time, more complex designs emerged, including multi-corner tubes, filled tubes [16], multi-cell structures [17], [18], and filled multi-cell tubes [19]. Furthermore, the latest developments include bio-inspired structures, where the design configurations are inspired by natural structures. An example of such research is the work conducted by Zhang et al. [20].

Extending this exploration of design evolution, various configurations have led to the establishment of a reference for creating specimens with hybrid structures consisting of circular tubes and multi-cell tubes [21]. This progression is motivated by the benefits of hybrid structures, which aim to enhance the material properties and crashworthiness values through the combination of two or more different materials. As research continues to advance, the focus has shifted towards hybrid cellular structures, which have garnered significant attention due to their advantageous features. According to G. Sun et al. [22], the advantages of hybrid cellular structures include the ability to improve material performance, enhance stable energy absorption capabilities, and simultaneously have lower density, resulting in a lighter mass compared to hybrid metal.

Research utilizing the Fused Deposition Modeling (FDM) method has been extensively conducted and proven to play a role as an energy absorber, enhancing crashworthiness values [23]. This method offers numerous advantages and ease in the specimen manufacturing process. It is known for its simplicity, requiring no molds and expensive tooling equipment, making the manufacturing process more straightforward. The Al/Nylon66 hybrid tube absorbed 380.76 J of energy, with a specific energy absorption (SEA) of 8.59 J/g.

Similar research has been conducted by X. Fu et al. [24] and Dony et al. [25] using the Hybrid Multi-Cell configuration. In X. Fu et al.'s study [24], a hybrid investigation delved further into crashworthiness performance through numerical simulations. The results obtained are that the Force-Displacement curve increases 28,4% along with increasing thickness variations. Dony et al . [25] conducted research using a specimen structure configuration tested under quasi-static loading, involving a combination of AL, PLA (shell), and PLA (core). The results of the research indicated that the Hybrid PLAt–Al PLA specimen produced the highest values for Energy Absorption (428,01 J) and Crash Force Efficiency (0,77). However, a closer look at the Force-Displacement curve revealed only a slight increase in the difference in Fmax values (6,5%). This suggests that while the addition of a shell in the hybrid structure can enhance the Fmax value, the improvement obtained is relatively small. Therefore, further experimentation with varying shell thicknesses is needed.

This research aims to explore the crashworthiness performance of 3D-printed multi-cell hybrid tubes. The study involves varying the thickness of the shell and the filament used. The thickness of the shell is varied between 1; 1.5 and 2 mm, while the filament variations include PACF and PLA, with the geometric shape being a circular tube. This investigation is expected to unveil valuable knowledge regarding the optimization of crashworthiness in 3D-printed structures hybrid tubes, fostering advancements in design and material selection strategies.

2. Methods

The materials employed in this study consisted of Polylactid Acid (PLA) filament, Polyamide and Carbon Fiber (PA-CF) filament, and aluminum tubes. All filaments were sourced from Shenzhen ESun Industrial and exhibited a diameter of 1.75 mm. The mechanical properties of the filament and aluminum are shown in **Table 1**.

The test specimen is a hybrid tube configuration consisting of shell-Al-multi cell, **Figure 1**. The shell and multi cell structures are printed using the fused deposition modeling method with a Creality 3D printer. The parameters of the printing process are shown in **Table 2**.

Table 1. Specimen material properties [26], [27]

Properties	PLA	PACF	Al
Density (g/cm³)	1.24	1.24	2.7
Tensile Strength (MPa)	20-30	140	90-400
Elongation at Break (%)	5-10	10,61	10-40
Flexural Strength (MPa)	101.2	140	150-300
Flexural Modulus (MPa)	3118.8	4363	70-75
Izod Impact Strength (kJ/m²)	3.09	18,67	30-100

Table 2. Parameter for manufacturing shell and multi cell

Parameter	PLA	PACF
Nozzle temperature (°C)	205	240
Platform temperature (°C)	60	80
Printing speed (mm/s)	60	60
Fill density (%)	100	100
Layer height (mm)	0,1	0,1

An aluminum tube with a diameter of 1 inch is employed as the second-layer structure in the hybrid configuration. The specimen's length is determined based on the length-to-diameter ratio (L/d = 2). The aluminum tube serves as the crush initiator because it has a slightly different length compared to the 3D printer specimen. The global peak crushing force (GPCF) can occur in Multi-Cell tube specimens with an initiator at the end or in Multi-Cell specimens with a tapered end [28]. The multi-cell was manufactured with an outer diameter of 24.3 mm and a thickness of 1 mm, creating an interference fit with the inner diameter of the aluminum tube. This interference fit was achieved by applying a manual compressive force to insert the multi-cell into the aluminum tube. Following the same principle as the multi-cell, the shell was designed with a matching inner diameter of 25.4 mm and thickness of 1; 1.5 & 2 mm to ensure fit within the aluminum component. The assembly method involved a manual press-fit, mirroring the process used for the multi-cell.

A total of six shell thickness variations were tested, each represented by five samples, resulting in five data sets for each variation. This approach was adopted to improve the precision of the research findings.

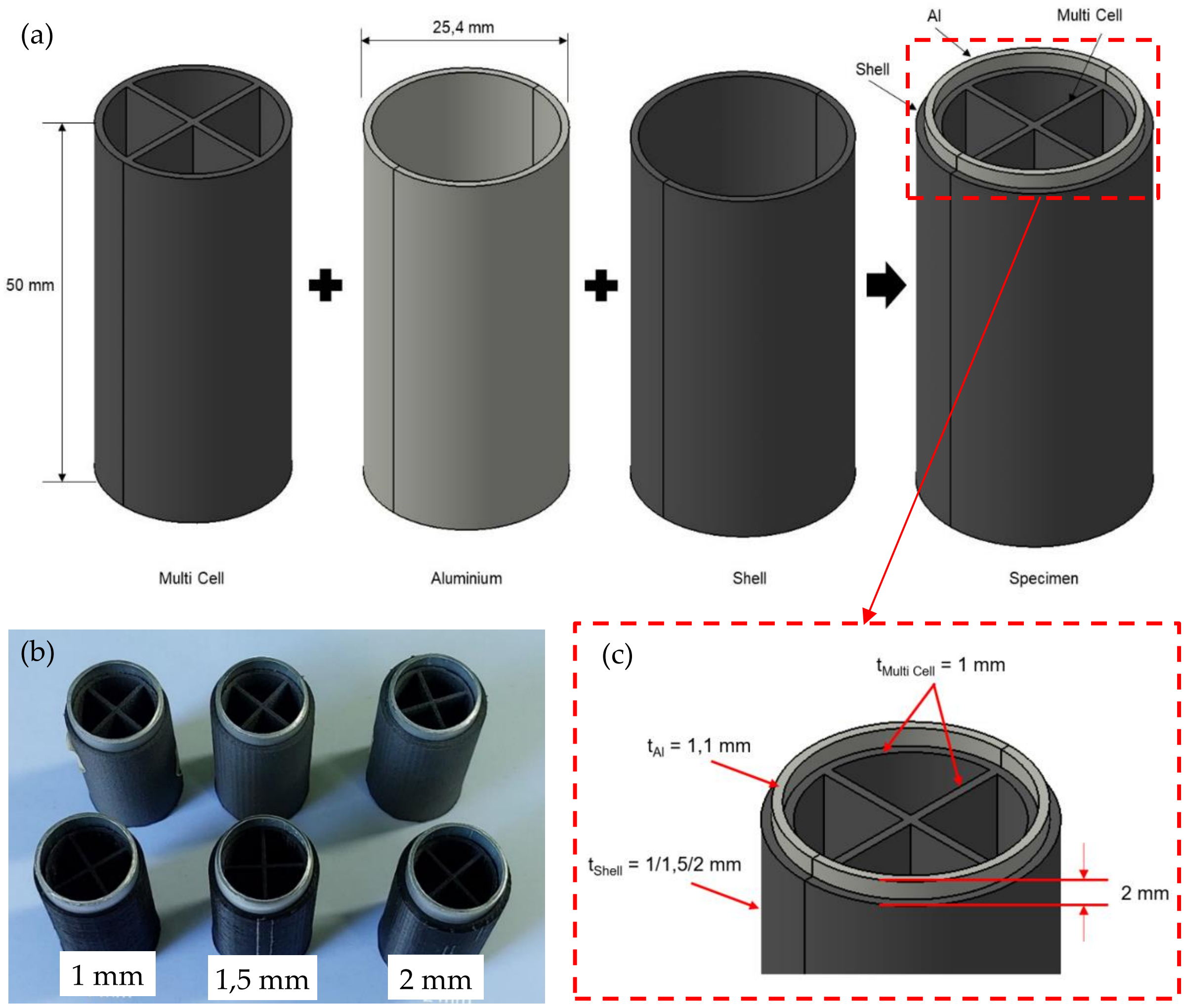

Figure 1. Specimen preparation (a) sequence of processes; (b) hybrid tube specimens; (c) specimens dimension

Table 3. Specimen mass

Specimen	Shell Thickness (mm)	Mass (gr)
PACF 1	1	19.6
PACF 1.5	1.5	21.8
PACF 2	2	25.4
PLA 1	1	20.6
PLA 1.5	1.5	23.6
PLA 2	2	27.1

The hybrid tube specimens conducted axial quasi-static compressive tests, as shown in Figure 2, using a tensilon universal test machine (UTM) at a speed of 5 mm/min to examine their crushing behaviors. The tests were conducted at the Materials Testing Laboratory, Research Center of Aeronautics Technology, ORPA, BRIN. The instantaneous force data from this experiment were compared to the displacement data of the specimen induced by compressive loading. Throughout the testing procedure, images of the specimens were also taken in order to analyze their crashworthiness characteristics. It was decided to observe the deformation process for both filament variations (PLA and PACF) until a displacement of 30 mm, which corresponds to 60% of the tube length [28] rather than 2/3 of the tube length [29]. This decision was made to standardize the specimen calculations.

Typical crashworthiness measures including F_{max}, F_{avg}, E_a, SEA and CFE are used to evaluate the specimen's crashworthiness. The F_{max} value can be observed in the Force-Displacement curve in the Initial Peak Crushing Force (IPCF) value which

Figure 2. The experimental setup for quasi-static compression testing

occurs in the pre-crushing stage. However, for specimens with a multi-cell configuration and the crush initiator Fmax used is Global Peak Crushing Force (GPFC) [28]. This GPCF value is obtained by looking for the overall/global peak value produced by the Force-Displacement curve during the axial quasi static testing process. Other parameters, such energy absorption (E_a), can be determined using the following formula:

$$E_a = \int_0^{D_{max}} F(x)dx. \quad (1)$$

Where, the energy absorption (E_a) of a specimen is obtained from the area under the curve.

Meanwhile, F_{avg} is obtained from E_a divided by the maximum displacement (D_{max}):

$$F_{mean} = \frac{E_a}{D_{max}} \quad (2)$$

While crush force efficiency (CFE) is the ratio of F_{avg} and F_{max}. If the CFE value is near to 1, it is considered optimal.

$$CFE = \frac{F_{mean}}{F_{max}} \quad (3)$$

And specific energy absoprtion (SEA) is generally used to assess the energy absorption capability per unit mass.

$$SEA = \frac{E_a}{m} \quad (4)$$

3. Results and Discussion

3.1. *Hybrid Tube Crashworthiness*

Figure 3 shows the average force-displacement curves of PACF and PLA specimens with various shell thickness. From the comparison of the two graphs, it appears that PLA generates a greater reaction force than PACF, indicating higher energy absorption. The Initial Peak Crushing Force (IPCF) values for both materials are not significantly different, but for PLA, the Global Peak Crushing Force (GPFC) is much higher, by approximately 70%. In the case of PLA, the reaction force continues to increase on the second and third folds before eventually decreasing on the fourth fold. For both specimens, it can be observed that the reaction force increases proportionally with the increase in thickness, consistent with previous research [30].

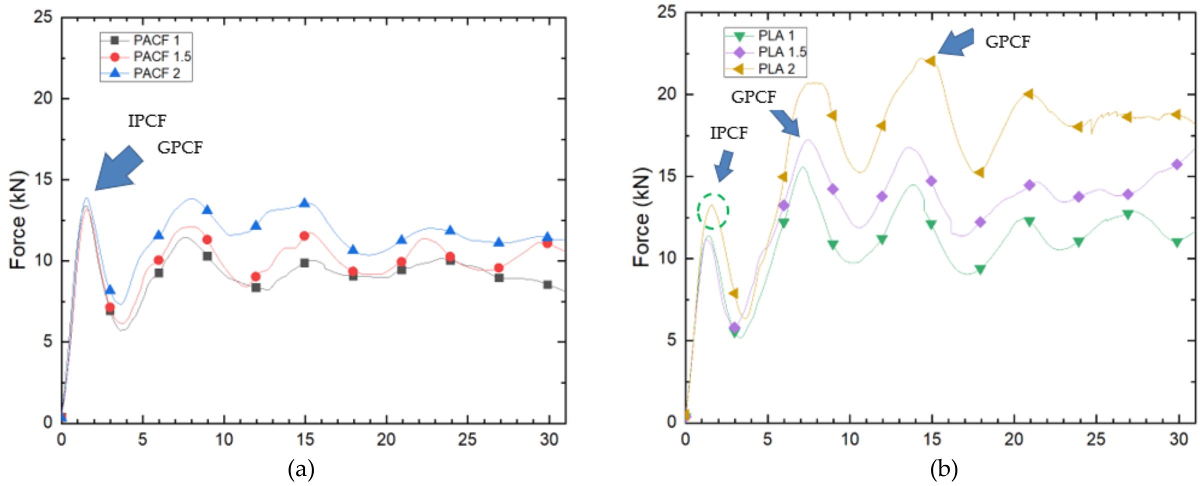

Figure 3. Force – displacement comparison of collapse tubes with different thickness: (a) PACF, and (b) PLA

The PLA specimen's average force-displacement curve is shown in **Figure 3b**. From the curve it can be seen that the first peak (IPCF) is formed which is circled in green. This peak indicates the presence of folds formed in the crush initiator (Al tube). Afterwards, another peak appears on the curve, its peak value surpassing the height of the initial peak. In the second peak, the specimen test process has hit the multi-shell and shell sections, which has resulted in the second peak and so on tending to increase. This is what differentiates between PLA and PACF, the first PLA peak is not GPCF. GPCF occurs after IPCF.

3.2. *Deformation Mode Analysis*

The force-displacement curve and the PACF specimen's deformation trend are shown in **Figure 4**. The deformation patterns of the three variations in specimen thickness tend to have almost the same pattern. The first circle mark (**Figure 4**), peak 1 on the curve indicates the formation of the first fold that hits Al as a crush initiator which occurs at a displacement of 2 mm. The second circle shows that the force value absorbed by the specimen decreases quite drastically at a displacement of 4 mm. The third circle, the second peak indicates the load starting to hit the shell, AL and multi-cell configuration structures. The fourth circle, the third peak forms the third fold, with a displacement of around 15 mm. From the third fold, it becomes increasingly visible that all PACF specimens experience a progressive mode in the form of a diamond mode. The fifth circle, the fourth peak forms the fourth fold by forming a diamond mode, which occurs at a displacement of 20-25 mm. The 6th circle, the fifth peak forms the fifth fold by forming a diamond mode as well, which occurs at a displacement of 30 mm.

An image of the PACF specimen post testing is shown in **Figure 5**. PACF specimen makes the specimen deform to form a mixed deformation

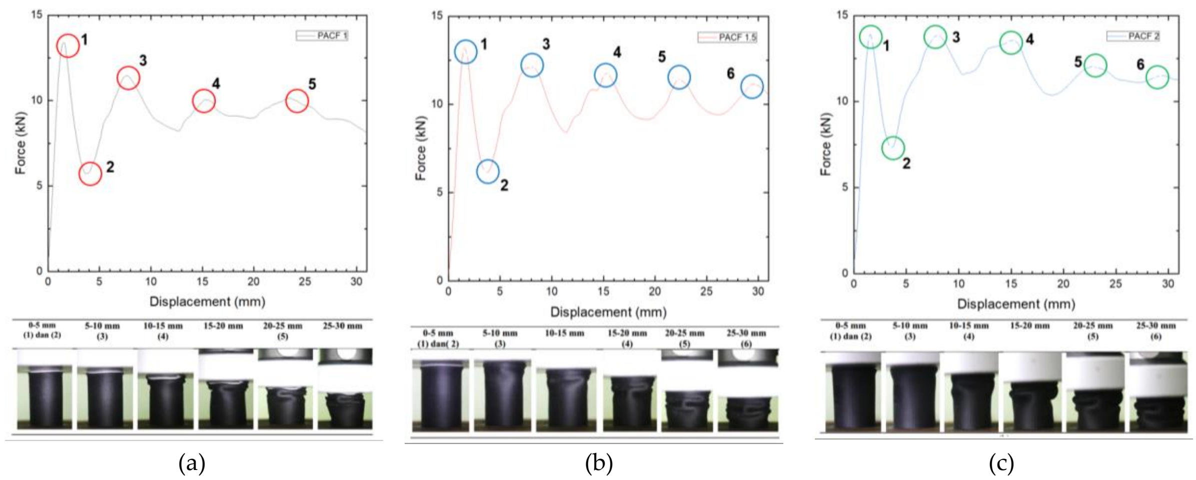

Figure 4. PACF deformation progress: (a) 1 mm; (b) 1.5 mm; and (c) 2 mm

(a) (b) (c)

Figure 5. PACF specimen post testing: (a) 1 mm; (b) 1.5 mm; and (c) 2 mm

mode. The Al structure which acts as a crush initiator becomes the structure that deforms first during testing. Deformation of the Al structure triggers other hybrid structures to deform according to the diamond mode. Along with to the diamond mode, the shell layer also forms a fracture mode. Medium-sized and larger fractures on the surface of the fold that experiences diamond mode exhibit the fracture mode. The fracture caused by the PACF 2 specimen experienced was the biggest when compared to the PACF 1 mm and 1.5 mm.

Figure 6 shows the force-displacement curve as well as the deformation trend of the PLA specimen. At the first peak, the first circle mark (Figure 6), the PLA condition is the same as PACF, namely a first fold that hits Al as a crush initiator occurs. The second circle shows that the loading force on the specimen decreases. Apart from that, at this moment fractured shell begins to occur at a thickness of 1 and 1.5 mm. The third circle, the second peak, indicates that the PLA 1 shell has broken, PLA 1,5 and PLA 2 have fractured.

Meanwhile, Al is seen deforming to form a diamond mode. The fourth circle, the third peak indicates the formation of the third fold which occurs at a displacement of 15 mm. From the image, it can be seen that the formation of this third fold makes the fragmented mode experienced in the PLA 1 specimen shell become wider. The fifth circle, fourth peak on the curve indicates the formation of the fourth fold which occurs at a displacement of 20 mm. From the figure, it can be seen that when the fourth fold is formed, the PLA 1 shell forms fragments that become even wider. The sixth circle, fifth peak indicates the formation of the fifth fold in the PLA specimen which occurs at a displacement of around 27 mm. The formation of this fifth fold resulted in the shell of the PLA 1 specimen breaking, the fragmented mode became wider and the PLA 1 shell no longer enveloped the Al tube so that the structure of the PLA 1 specimen was left with only Al and multi-cells which were still fused.

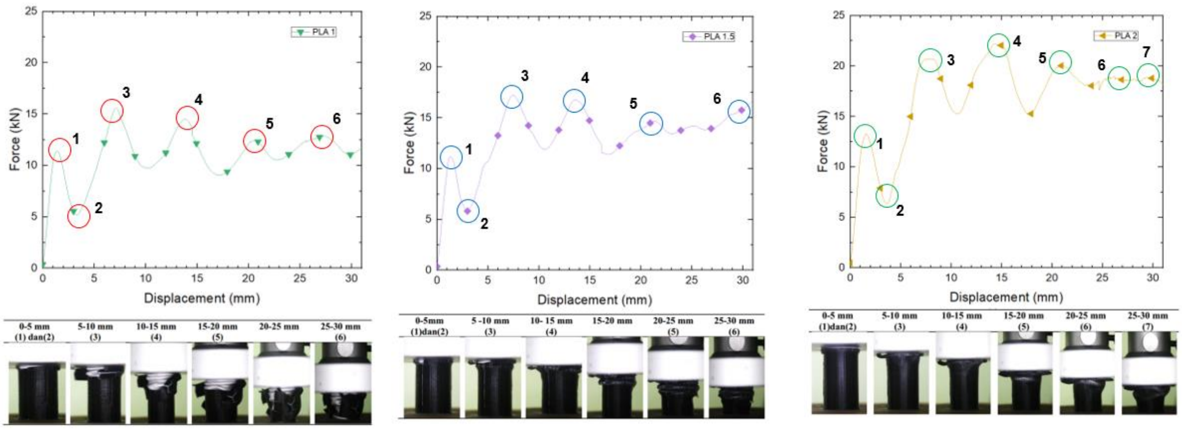

(a) (b) (c)

Figure 6. PLA deformation progress (a) 1 mm; (b) 1.5 mm; and (c) 2 mm

Figure 7 displays the PLA specimen post testing with different thickness. From the figure, it can be seen that the quasi-static impact test carried out on the PLA 1 specimen caused the specimen form a mixed deformation mode. In Al and multi-cell a diamond mode is formed, but in the shell structure it is deformed to form a fracture and fragmented mode. The fragments that formed caused the shell of the PLA 1 mm specimen (Figure 7a) to break vertically, starting from the top end of the tube to the bottom end of the tube. One of the PLA 1 mm specimens had such severe fragmentation and detached from the Al tube. Meanwhile, in PLA 1.5 mm (Figure 7b) the extensional folding mode is happened. The white streak appear in the folding location indicated the phenomena of plastic deformation.

The fragmented mode experienced only occurred at the top end of the PLA 1.5 mm specimen and the number of fragments formed was not as much as the PLA 1 mm specimen. Besides that, PLA 2 mm (Figure 7c) also forms fracture and fragmented modes. Fragmented mode is indicated by the formation of fractures in the shell structure. The fragments that were experienced were large enough so that it appeared that the shell was covering the Al tube imperfectly.

3.3. *Energy Absorption*

Figure 8 present a comparative analysis of the energy absorption characteristics of PACF and PLA materials under compressive loading. Both material types demonstrate a positive correlation between displacement and energy absorption, indicating that the materials can absorb energy through deformation. The graph shows that the specimen's energy absorption value rises with increasing shell thickness. Wall thickness directly impacts the value of absorbed energy [31]. Tubes with thicker walls tend to experience higher peak loads [27]. Thicker surfaces lead to larger specimen volumes, necessitating greater energy input to overcome atomic bond resistance and induce plastic deformation upon impact.

However, the PLA materials consistently exhibit higher energy absorption values compared to the PACF materials suggesting that PLA may be a more suitable candidate for applications requiring high energy absorption. In PACF specimens there was an increase of 7.5% from a thickness of 1 mm to 1,5 mm. In the meantime, there has been a 24% rise in thickness from 1 to 2 mm. The PLA data display a steeper linear trend compared to the PACF data: energy absorption increased by 54% from 1 mm to 2 mm thickness, while it increased by only 19% from 1 mm to 1.5 mm thickness.

A comparison of the Energy Absorption (ES) values for each thickness variation can be seen in Figure 9. The largest energy absorption occurred in the PLA 2 specimen at 504 J. Meanwhile, the smallest energy absorption is in the 1 mm PACF specimen, namely 275,6 J. Similar to Figure 8, both PLA and PACF exhibited a general trend of increasing energy absorption with increasing thickness. However, the rate of increase in energy absorption per unit thickness was not linear. At all thicknesses, PLA consistently demonstrated higher energy absorption values compared to PACF. Specifically, PLA exhibited an 18.97% higher energy absorption at 1 mm thickness (275.6 J vs. 327.9 J), which increased to 31.54% at 1.5 mm thickness (296.3 J vs. 389.7 J). The most significant difference was observed at 2 mm thickness, with PLA exhibiting 46.84% higher energy absorption (342.9 J vs. 504 J).


(a)


(b)


(c)

Figure 7. PLA specimen post testing: (a) 1 mm; (b) 1.5 mm; and (c) 2 mm

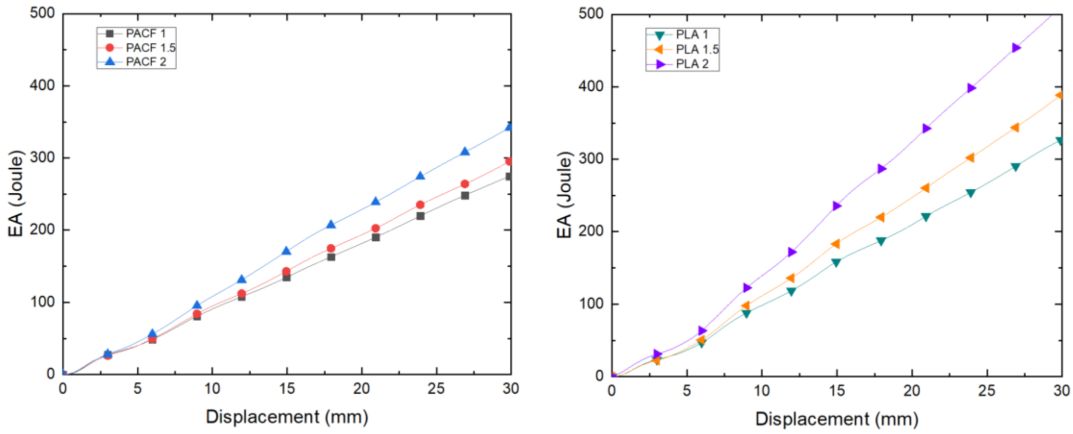

(a) (b)

Figure 8. EA-Displacement curve : (a) PACF & (b) PLA

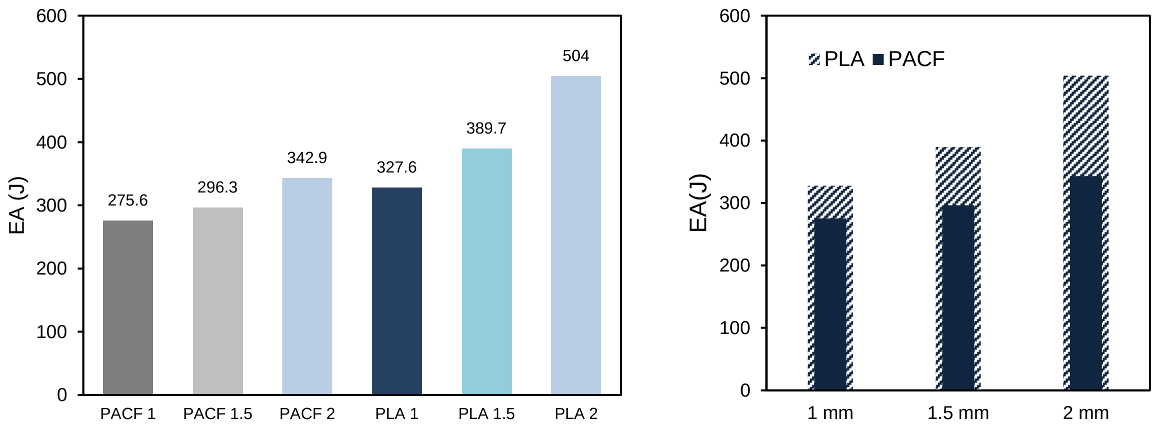

Figure 9. Comparison of Energy Absorption (EA) values for each thickness variation (a) all specimens and (b) PLA vs PACF specimens

3.4. Specific Energy Absorption and Crushing Force Efficiency

Based on Equation (4), the mass unit value has an inverse relationship with the SEA value, whereas the SEA value is directly proportional to the EA value. The specimen's unit mass value must be as low possible and the energy absorption value must be large in order to get the best SEA value.

Comparing the SEA and CFE values of PLA and PACF specimens as the thickness variation increases is shown in Figure 10. From the bar diagram, it can be seen that in PACF specimens, as the thickness increases, the SEA value decreases. The SEA PACF 1 value is 14.05 J/g to 13.58 J/g at a thickness of 1.5 and decreases again at a thickness of 2 mm to 13.52 J/g. On the other hand, for PLA specimens, when the shell thickness was increased, the A value increased by 17% when the shell thickness was 2 mm (15.87 J/g to 18.61 J/g), and increased by 4% when the shell thickness was 1.5 mm (15.87 J/g to 16.53 J/g). Due to PLA's brittle, highly stiff nature and its high compressive strength, the area under the curve increases, leading to higher values for EA and SEA [32].

Crush force efficiency (CFE) is the final parameter to be investigated. CFE is a parameter used to calculate the ratio between Mean Crushing Force (Favg) and Global Peak Crushing Force (GPCF) as stated in equation 3. The ideal CFE value is 1 or close to 1. If there is little difference between the GPCF value and the Favg value or the force-displacement curve tends to be stagnant and has stable peak-peak fluctuations, a CFE value of 1 may arise.

Empirical data analysis indicates a positive linear correlation between shell thickness and CFE values in both PACF and PLA specimens. These findings are consistent with the hypothesis that increasing the outer dimensions of the specimens will enhance compressive load capacity [33]. The increase in CFE values was significantly greater in PACF specimens compared to PLA specimens as the shell thickness increased. In PACF specimens, the CFE value increased by 19% when the thickness was 2 mm and 9% when the thickness was 1.5 mm. In PLA, the CFE value increases by 9% when the thickness is 2 mm and 7% when the thickness is 1.5 mm. PACF specimens, composed of polyamide filaments reinforced with carbon fiber (CF), exhibit superior CFE performance compared to PLA specimens. This enhanced performance is attributed to the CF reinforcement, which imparts properties similar to aluminum [34]. As evidenced by the force-displacement curves in **Figure 3**, PACF specimens demonstrate more stable peak fluctuations during deformation, further highlighting their superior CFE characteristics. Material selection is crucial for optimizing CFE values, as material type is the most influential parameter compared to other factors [17].

Figure 11 shows the relationship between Specific Energy Absorption (SEA) and Crush Force Efficiency (CFE). PLA exhibited significantly higher specific energy absorption (SEA) values compared to PACF, indicating its superior energy absorption capacity. However, PLA also required a greater crush force efficiency (CFE) to achieve this energy absorption, suggesting a more ductile failure mode. This behavior can be attributed to the higher degree of crystallinity and longer chain molecules in PLA, which enhance its ability to dissipate energy through plastic deformation.

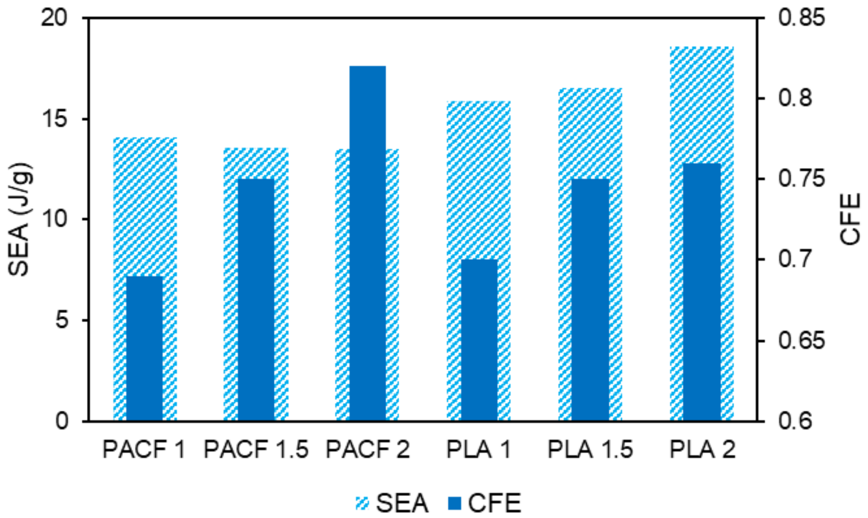

Figure 10. Comparison of SEA and CFE values of PACF and PLA specimens when thickness variations are increased

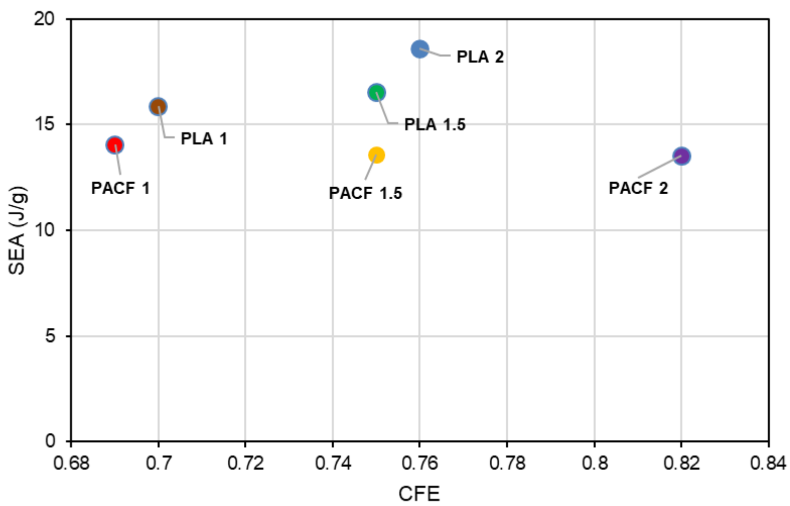

Figure 11. Specimen CFE – SEA Curve

4. Conclusion

The experimental study to determine the crashworthiness characteristics of 3D-printed tubes hybridized with aluminum has been successfully conducted. The two materials used, PACF and PLA, have different characteristics in terms of energy absorption and compression force efficiency. For all materials, the CFE value increased with the specimen thickness. Meanwhile, energy absorption was influenced not only by thickness but also by the failure mode during the experiment. In PLA material, the SEA value increased with thickness, but in PACF, the SEA value slightly decreased in thicker specimens.

The PACF specimen experienced diamond mode and fracture mode. And as the variation in shell thickness increases, the fractures that form become larger. Meanwhile, the PLA specimen experienced diamond, fracture and fragmented modes. The fragmented mode is happened in higher thickness. The more complex failure mode in tubes with PLA filament indicates better energy absorption compared to PACF.

The findings from this study contributes for the selection of materials in applications of energy absorption for rapid use. For instance, PLA materials may be well-suited for use in protective equipment or packaging materials. Further research on the use of adhesive between PLA and aluminum is of interest as a means to enhance bonding and load transfer between the two materials, with the aim of achieving better performance. Other tests, such as oblique impact testing, also present an interesting topic for exploration.

Acknowledgments

The authors thank the facilities and technical support from Aeronautics Laboratories Rumpin, National Research and Innovation Agency through E-Layanan Sains-BRIN. This work is supported by the project of "Study of Crashworthiness Aspects in Aircraft Structures to Enhance Transportation Safety" No.27/III.1/HK/2024 under the grant of research Organization for Aeronautics and Space of National Research and Innovation Agency (BRIN), Bogor, Indonesia.

Author's Declaration

Authors' contributions and responsibilities

The authors made substantial contributions to the conception and design of the study. The authors took responsibility for data analysis, interpretation and discussion of results. The authors read and approved the final manuscript.

Funding

This research is funded by Research Center for Aeronautics Technology, National Research and Innovation Agency – BRIN.

Availability of data and materials

All data are available from the authors.

Competing interests

The authors declare no competing interest.

Additional information

No additional information from the authors.

References

[1] T. Taki, M. Machida, and R. Shimada, "Trends of traffic fatalities and DNA analysis in traffic accident investigation," *IATSS research*, vol. 43, no. 2, pp. 84–89, 2019, doi: 10.1016/j.iatssr.2019.05.001.

[2] S. I. Mohammed, "An Overview of Traffic Accident Investigation Using Different Techniques," *Automotive Experiences*, vol. 6, no. 1, pp. 68–79, Jan. 2023, doi: 10.31603/ae.7913.

[3] M. Mutharuddin *et al.*, "The Road Safety: Utilising Machine Learning Approach for Predicting Fatality in Toll Road Accidents," *Automotive Experiences*, vol. 7, no. 2, pp. 236–251, 2024, doi: 10.31603/ae.11082.

[4] N. Md Yusof *et al.*, "Effect of Road Darkness on Young Driver Behaviour when Approaching Parked or Slow-moving Vehicles in Malaysia," *Automotive Experiences*, vol. 6, no. 2, pp. 216–233, May 2023, doi: 10.31603/ae.8206.

[5] W. A. Al Bargi, M. M. Rohani, B. D. Daniel, N. A. Khalifaa, M. I. M. Masirin, and J. Kironde, "Estimating of Critical Gaps at Uncontrolled Intersections under Heterogeneous Traffic Conditions," *Automotive Experiences*, vol. 6, no. 2, pp. 429–437, 2023, doi: 10.31603/ae.9406.

[6] E. Yong *et al.*, "Investigation of the Vehicle Driving Trajectory During Turning at Intersectional Roads Using Deep Learning Model," *Automotive Experiences*, vol. 7, no. 1,

pp. 63–76, Apr. 2024, doi: 10.31603/ae.10649.

[7] W. Artha Wirawan, A. Zulkarnain, H. Boedi Wahjono, Jamaludin, and A. Tyas Damayanti, "The Effect of Material Exposure Variations on Energy Absorption Capability and pattern of Deformation Material of Crash Box of Three Segments," *Journal of Physics: Conference Series*, vol. 1273, no. 1, 2019, doi: 10.1088/1742-6596/1273/1/012081.

[8] F. Djamaluddin, S. Abdullah, A. K. Ariffin, and Z. M. Nopiah, "Optimization of foam-filled double circular tubes under axial and oblique impact loading conditions," *Thin-Walled Structures*, vol. 87, pp. 1–11, 2015, doi: 10.1016/j.tws.2014.10.015.

[9] A. Jusuf, T. Dirgantara, L. Gunawan, and I. S. Putra, "International Journal of Impact Engineering Crashworthiness analysis of multi-cell prismatic structures," vol. 78, pp. 34–50, 2015.

[10] Y. Zhang *et al.*, "Crashworthiness design of car threshold based on aluminium foam sandwich structure," *International Journal of Crashworthiness*, vol. 27, no. 4, pp. 1167–1178, 2022, doi: 10.1080/13588265.2021.1914978.

[11] A. R. Zubir, K. Hudha, Z. A. Kadir, and N. H. Amer, "Enhanced Modeling of Crumple Zone in Vehicle Crash Simulation Using Modified Kamal Model Optimized with Gravitational Search Algorithm," *Automotive Experiences*, vol. 6, no. 2, pp. 372–383, Aug. 2023, doi: 10.31603/ae.9289.

[12] T. Zhu *et al.*, "Rail vehicle crashworthiness based on collision energy management: an overview," *International Journal of Rail Transportation*, vol. 9, no. 2, pp. 101–131, 2021, doi: 10.1080/23248378.2020.1777908.

[13] H. Mou, J. Xie, Y. Liu, K. Cheng, and Z. Feng, "Impact test and numerical simulation of typical sub-cargo fuselage section of civil aircraft," *Aerospace Science and Technology*, vol. 107, 2020, doi: 10.1016/j.ast.2020.106305.

[14] Y. G. Ko, S. J. Kim, and J. K. Paik, "Effects of a deformable striking ship's bow on the structural crashworthiness in ship–ship collisions," *Ships and Offshore Structures*, vol. 13, pp. 228–250, 2018, doi: 10.1080/17445302.2018.1442115.

[15] A. Baroutaji, M. Sajjia, and A. G. Olabi, "On the crashworthiness performance of thin-walled energy absorbers: Recent advances and future developments," *Thin-Walled Structures*, vol. 118, no. April, pp. 137–163, 2017, doi: 10.1016/j.tws.2017.05.018.

[16] G. Sun, S. Li, Q. Liu, G. Li, and Q. Li, "Experimental study on crashworthiness of empty/aluminum foam/honeycomb-filled CFRP tubes," *Composite Structures*, vol. 152, pp. 969–993, 2016, doi: 10.1016/j.compstruct.2016.06.019.

[17] D. Hidayat *et al.*, "Investigation on the Crashworthiness Performance of Thin-Walled Multi-Cell PLA 3D-Printed Tubes: A Multi-Parameter Analysis," *Designs*, vol. 7, no. 5, 2023, doi: 10.3390/designs7050108.

[18] Y. Liu *et al.*, "Effects of loading rate and temperature on crushing behaviors of 3D printed multi-cell composite tubes," *Thin-Walled Structures*, vol. 182, no. October 2022, p. 110311, 2023, doi: 10.1016/j.tws.2022.110311.

[19] G. Sun, T. Liu, X. Huang, G. Zhen, and Q. Li, "Topological configuration analysis and design for foam filled multi-cell tubes," *Engineering Structures*, vol. 155, no. October 2017, pp. 235–250, 2018, doi: 10.1016/j.engstruct.2017.10.063.

[20] L. Zhang, Z. Bai, and F. Bai, "Crashworthiness design for bio-inspired multi-cell tubes with quadrilateral, hexagonal and octagonal sections," *Thin-Walled Structures*, vol. 122, no. June 2017, pp. 42–51, 2018, doi: 10.1016/j.tws.2017.10.010.

[21] Z. Zhang, Q. Liu, J. Fu, and Y. Lu, "Parametric study on the crashworthiness of the Al/CFRP/GFRP hybrid tubes under quasi-static crushing," *Thin-Walled Structures*, vol. 192, no. June, 2023, doi: 10.1016/j.tws.2023.111156.

[22] G. Sun, D. Chen, G. Zhu, and Q. Li, "Lightweight hybrid materials and structures for energy absorption: A state-of-the-art review and outlook," *Thin-Walled Structures*, vol. 172, no. December 2021, 2022, doi: 10.1016/j.tws.2021.108760.

[23] X. Fu, X. Zhang, and Z. Huang, "Axial crushing of Nylon and Al/Nylon hybrid tubes by FDM 3D printing," *Composite Structures*, vol. 256, no. June 2020, 2021, doi:

10.1016/j.compstruct.2020.113055.

[24] X. Fu, X. Zhang, and Z. Huang, "Axial crushing of Nylon and Al/Nylon hybrid tubes by FDM 3D printing," *Composite Structures*, vol. 256, p. 113055, 2021, doi: https://doi.org/10.1016/j.compstruct.2020.113055.

[25] D. Hidayat *et al.*, "Experimental investigation on axial quasi-static crushing of Al/PLA hybrid tubes," *Journal of Physics: Conference Series*, vol. 2551, no. 1, 2023, doi: 10.1088/1742-6596/2551/1/012008.

[26] "Properties Material." https://www.esun3d.com/pla-basic-product/.

[27] M. B. Azimi and M. Asgari, "A new bi-tubular conical-circular structure for improving crushing behavior under axial and oblique impacts," *International Journal of Mechanical Sciences*, vol. 105, no. November, pp. 253–265, 2016, doi: 10.1016/j.ijmecsci.2015.11.012.

[28] H. Yin, H. Fang, Y. Xiao, G. Wen, and Q. Qing, "Multi-objective robust optimization of foam-filled tapered multi-cell thin-walled structures," *Structural and Multidisciplinary Optimization*, vol. 52, no. 6, pp. 1051–1067, 2015, doi: 10.1007/s00158-015-1299-8.

[29] K. Wang, Y. Liu, J. Wang, J. Xiang, S. Yao, and Y. Peng, "On crashworthiness behaviors of 3D printed multi-cell filled thin-walled structures," *Engineering Structures*, vol. 254, p. 113907, 2022, doi: https://doi.org/10.1016/j.engstruct.2022.113907.

[30] W. A. Wirawan, B. Junipitoyo, S. H. S. Putro, A. H. Suudy, R. Ridwan, and M. A. Choiron, "Collapse Behavior and Energy Absorption Characteristics of Design Multi-Cell Thin Wall Structure 3D-Printed Under Quasi Statistic Loads," *Automotive Experiences*, vol. 7, no. 1, pp. 149–160, 2024, doi: 10.31603/ae.10892.

[31] D. Hidayat *et al.*, "Experimental Study on Crashworthiness Characteristics of Composite Hybrid Tube Utilise Axial Quasi-Static Crushing Test," *AIP Conference Proceedings*, vol. 2941, no. 1, 2023, doi: 10.1063/5.0181353.

[32] L. Ranakoti *et al.*, "Critical Review on Polylactic Acid: Properties, Structure, Processing, Biocomposites, and Nanocomposites," *Materials*, vol. 15, no. 12, 2022, doi: 10.3390/ma15124312.

[33] E. Cetin, "Energy absorption of thin-walled multi-cell tubes with DNA-inspired helical ribs under quasi-static axial loading," *Journal of the Brazilian Society of Mechanical Sciences and Engineering*, vol. 46, no. 10, pp. 1–19, 2024, doi: 10.1007/s40430-024-05181-6.

[34] S. Shashikumar and M. S. Sreekanth, "Investigation on mechanical properties of polyamide 6 and carbon fiber reinforced composite manufactured by fused deposition modeling technique," *Journal of Thermoplastic Composite Materials*, vol. 37, no. 5, pp. 1730–1747, Sep. 2023, doi: 10.1177/08927057231200006.